Theory of Time-Resolved Photoelectron Imaging: Nonperturbative Calculation for an Internally Converting Polyatomic Molecule

Yoshi-ichi Suzuki,[1] Mauro Stener,[2] and Tamar Seideman[1,*]

[1]*Steacie Institute for Molecular Science, National Research Council of Canada, Ottawa, Ontario, Canada K1A OR6*
[2]*Dipartimento di Scienze Chimiche, Università di Trieste, Via L. Giorgieri 1, I-34127 Trieste, Italy*

(Received 27 July 2002; published 15 November 2002)

We present the first calculation of time-resolved photoelectron angular distributions for a polyatomic system. Our method takes rotations into exact account, treats the laser field nonperturbatively, and computes the electronic dynamics from first principles. Our results point to the information content of time-resolved photoelectron imaging observables and illustrate the role played by the field intensity.

DOI: 10.1103/PhysRevLett.89.233002 PACS numbers: 33.50.Hv, 33.60.Cv, 82.53.–k

Femtosecond time-resolved photoelectron imaging (PEI) is a young but rapidly growing subdiscipline of femtochemistry [1–6]. The time-resolved photoelectron image translates into the photoionization differential cross section, energy resolved to within the probe bandwidth. It thus provides both the energy and the angular distribution of the photoelectron as well as their correlation as a function of time. The reason for the increasing popularity of this probe technique [4] is the realization that time-resolved photoelectron angular distributions (PADs) contain a wealth of information that is not available from angle-integrated observables [3]. The rich information content of time-resolved PEI derives from an intricate combination of interferences in time and angular momentum spaces and therefore comes at a cost. Recent experimental studies have stressed the need for theory and modeling of time-resolved PADs to utilize the potential of time-resolved PEI.

The formalism for calculation of time-resolved photoelectron differential cross sections (and hence all the observables of PEI) was developed several years ago for linear systems [7] and was recently extended to apply to molecules of arbitrary symmetry [8]. For several reasons, however, numerical implementation remains a challenge. An exact account of angular momentum algebra is essential, nonperturbative treatment of the pump field is typically necessary, and a proper account of the ionization dynamics is often required. Thus, all time-resolved calculations to date have been restricted to diatomic molecules. Since, however, time-resolved PEI is intended as a probe of systems whose properties are unknown, one is typically interested in exploring complex polyatomic systems. These are also the systems that are convenient to excite and ionize in the laboratory and the ones of relevance to modeling of photobiological processes and to the design of future devices [2,3,6,9].

Here we present the first calculation of time-resolved PADs for a polyatomic molecule. We consider the dynamics of an ultrafast nonradiative transition, since these dynamics and their variety of applications have been the focus of much of the time-resolved photoelectron spectroscopy literature [2,6]. From a numerical viewpoint, this application is particularly challenging due to the involvement of two excited electronic states and a large density of vibrational levels. Our results point to the information content of PEI, suggesting an observable, derivable from PEI, that maps the electronic population dynamics, effectively disentangling the electronic modes from the vibrational motion to which they are strongly coupled. We show also that the pump intensity plays a particularly interesting role in PEI experiments of nonradiative transitions.

The time-evolving wave packet is expanded in an eigenbasis of a zero order Hamiltonian that excludes the nonradiative electronic coupling and the field-matter interaction, leading to a set of coupled differential equations for the expansion coefficients that are solved numerically. The photoelectron differential cross section, and several observables derived from it, is computed using the formalism of [7,8]. The ionization matrix elements (the matrix elements of the dipole operator between the bound and free electronic states), which are input to the theory, are computed using the *ab initio* method of [10]. More details of the electronic structure and dynamical calculations will be published elsewhere.

The $(S_2 \rightarrow S_1)$ internal conversion of pyrazine serves as a convenient model. This system has been studied extensively by Domcke and co-workers, who computed high quality *ab initio* potential energy surface for the neutral and ionic states involved [11–15]. Experimental and numerical angle-integrated photoelectron studies of this conversion are reported in Refs. [16] and [11,12,15,17], respectively. Both models proposed in [12] are considered. Model A corresponds, within the independent electrons approximation, to the physical ionization propensities of pyrazine, where the optically dark (S_1) state correlates upon ionization with the electronic ground state of the cation, whereas the bright (S_2) state correlates with the first excited cation state. Within model B both states ionize into the ground state of the cation. The motivation for complementing the physical model with an artificial one is to derive more general

conclusions from the results, which will pertain to a variety of molecules.

For linearly polarized pump and probe fields with common polarization direction, the energy- and angle-resolved ionization signal is cylindrically symmetric [3],

$$\sigma(\Delta t, \bar{\epsilon}) = \frac{\sigma_{\rm tot}(\Delta t, \bar{\epsilon})}{4\pi} \sum_j \beta_{2j}(\Delta t, \bar{\epsilon}) P_{2j}(\cos\theta_k), \qquad (1)$$

where $\sigma_{\rm tot}(\Delta t, \bar{\epsilon})$ is the integral (time and energy-resolved) cross section, $\beta_0 = 1$, $\beta_{2j>0}(\Delta t, \bar{\epsilon})$ are asymmetry parameters, Δt is the time delay between the pump and probe pulses, $\bar{\epsilon}$ is the photoelectron energy, defined to within the probe bandwidth, and θ is the photoelectron scattering angle, defined with respect to the polarization vector. The energy-integrated PAD, $\sigma(\Delta t)$, takes the same functional form in terms of $\sigma_{\rm tot}(\Delta t)$ and $\beta_{2j}(\Delta t)$. The upper limit on the j summation in Eq. (1) is determined by the pump intensity and duration, as discussed below.

Whereas the integral cross section exhibits all time scales in the problem and is dominated by the vibrations, the asymmetry parameters respond only to the electronic and rotational dynamics, serving as an effective filter of the vibrations. In the weak field (golden rule) limit, only the lowest order moments of the angular distribution ($\beta_{2j},\ j \le 2$) are nonzero. The latter exhibit only the lowest order ($\Delta J = 2$) rotational coherences, corresponding to the time scales of rotational periods. On the short time scales typical of internal conversions, these coherences are not observed and hence the structure of $\beta_{2j},\ j = 1, 2$ is expected to reflect solely the electronic dynamics.

At nonperturbative pump intensities, the system cycles between the ground and optically bright states with a period Ω_R^{-1}, Ω_R being the Rabi coupling, exchanging a unit of angular momentum with the field on each transition [18]. The PAD probes sensitively the ensuing, coherent rotational wave packet dynamics. Higher moments ($\beta_{2j},\ j > 2$) become available, reflecting the higher moments of the wave packet alignment and providing new information. In the case of a nonradiative transition, the nonperturbative field induces in addition rotational interferences that are not observed in single excited state models, as illustrated below.

Figure 1 shows the asymmetry parameters derived from the energy-integrated PAD along with the diabatic population in the S_1 and S_2 states. The intensity is chosen sufficiently low for terms beyond the third in Eq. (1) to vanish. The inset in Fig. 1(a) shows the potential energy surfaces along the totally symmetric Q_{6a} coordinate. Evidently, $\beta_4(\Delta t, \bar{\epsilon})$ tracks faithfully the internal conversion dynamics in the case of model B [Fig. 1(b), dot-dashed curve]. Here the change of electronic symmetry of the bound state upon transition implies a change of the symmetry of the outgoing electronic wave [8,19], because the product of irreducible representations of the bound electronic state, the dipole operator, the free electronic

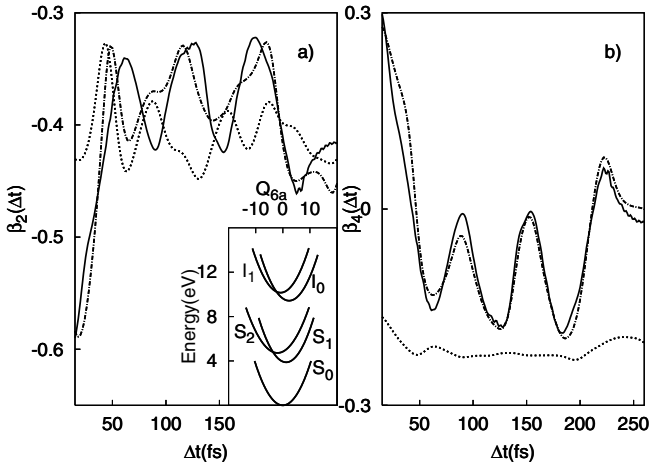

FIG. 1. Ionization symmetry parameters $\beta_{2j}(\Delta t),\ j = 1, 2$ derived from energy-integrated PADs for model A (dotted curves) and model B (dot-dashed curves) along with the diabatic population in the S_1 [panel (a)] and S_2 [panel (b)] states (solid curves). The inset in panel (a) gives the potential energy surfaces [13] along the totally symmetric Q_{6a} coordinate. Ground state pyrazine molecules are excited by a $2\sqrt{\ln 2}\tau_{\rm pu} = 1$ fs pump pulse and, subsequent to a delay time Δt, ionized by $2\sqrt{\ln 2}\tau_{\rm pr} = 15$ fs probe pulse. The pump intensity is chosen sufficiently low to eliminate rotational pumping. The pump energy is fixed at the $S_0 - S_2$ vertical excitation energy and the probe energy (7.89 eV) is chosen sufficiently large to ionize all populated vibrational levels of both S_1 and S_2 states.

state, and the ion electronic state must contain the totally symmetric representation. The mild alignment induced by the pump field in the weak pump limit suffices to translate the symmetry change with respect to the molecular axes into a dramatic change of the laboratory frame PAD [8,19,20], as summarized by the dot-dashed curve of Fig. 1(b).

We remark that the linearly polarized pump pulse induces only one-dimensional alignment; it aligns the body-fixed z axis to the polarization vector but does not hinder rotation in the two azimuthal angles (rotation about the body-fixed and space-fixed z axes). Depending on the sense of the pump-induced transition, this rotation may or may not degrade the sensitivity of the PAD to the population transfer. In the case of pyrazine and in the two cases explored previously [19,20] it does not, but we expect that in other systems it will. The possibility of hindering the rotations in all three Euler angles by means of a moderately-intense far-off-resonance pulse of elliptical polarizability is inviting. The ability of elliptically polarized fields to induce 3D alignment of polyatomic molecules was recently demonstrated [21]. The application of 3D alignment to enhance the sensitivity of time-resolved PADs remains to be investigated.

The behavior exhibited by the dotted curve of Fig. 1(b), corresponding to $\beta_4(\Delta t, \bar{\epsilon})$ for model A, has been

anticipated. Here the ion states with which the bright and dark states correlate differ in electronic symmetry and hence the symmetry of the departing electron waves does not change in the course of the transition, producing an essentially time-independent asymmetry parameter. Often it is possible to force the two coupled states to ionize into the ground state of the ion by choice of the probe wavelength. The ionization probability may, however, differ significantly for the two states.

Less anticipated, and rather discouraging, is the trend exhibited by $\beta_2(\Delta t, \bar{\epsilon})$ [Fig. 1(a)]. The energy dependence of the ionization matrix elements gives rise to significant energy dependence of the β_2 asymmetry parameter of the uncoupled diabatic states. As a result, whereas the time evolution of β_4 tracks the wave packet dynamics in the case of model B and is practically constant in the case of model A, β_2 for both models exhibits modulations. These are related to, but do not map, the population dynamics. In particular, the β_2 parameter obtained for model A is not essentially constant in time, as may have been expected. Thus, the asymmetry parameters derived from the energy-integrated PAD may exhibit structure that could be mistaken for, but does not mirror, the wave packet dynamics. This misleading structure is fully eliminated by deriving the asymmetry parameters from photoelectron images (i.e., from energy-resolved PADs). The last result is illustrated numerically and theoretically elsewhere but is also intuitive; at constant photoelectron energy, the energy dependence of the ionization matrix elements no longer plays a role.

In Fig. 2 we examine the extent to which the energy resolution of PEI could serve to convey information about the wave packet dynamics also in the unfavorable case of model A. Panels (a) and (b) give polar plots of the energy-resolved PAD for two models that are identical in energetics but differ in the ionization propensities. Panel (b) corresponds to model B. Panel (a) corresponds to a modification of model A, where we have altered the I_1 potential energy surface to assume the shape and origin of the I_0 potential energy surface. The symmetries are not altered and hence the coupled states ionize into ion states of different electronic symmetry and the symmetry of the departing electron waves does not change in the course of the internal conversion. In panel (c) we show the ionization asymmetry parameters corresponding to the polar plots of panels (a) and (b) along with the diabatic population in the S_2 state. The photoelectron energy in each plot is chosen at the peak of the energy distribution. For both models, the energy-resolved PAD mirrors faithfully the internal conversion dynamics. In the case of model A [Fig. 2(a)] this correspondence owes to the dependence of the ionization matrix elements on the photoelectron energy. The energy gap between the S_2 and S_1 states [see the inset of Fig. 1(a)] translates into a change of the photoelectron energy distribution in the course of the internal conversion. An observable change of the photoelectron

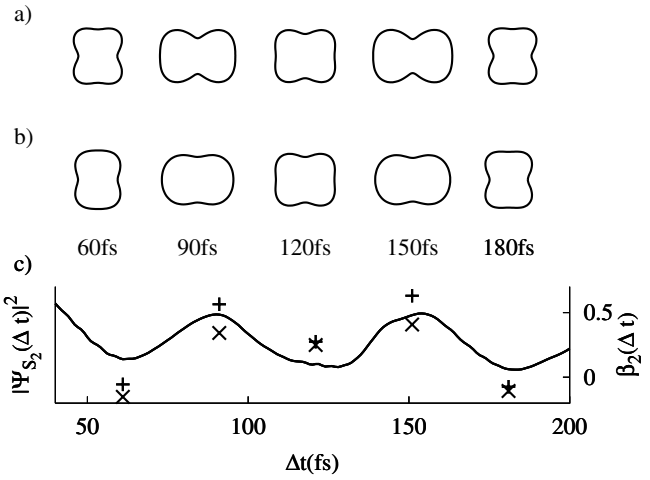

FIG. 2. Energy-resolved photoelectron angular distribution. Panels (a) and (b) show polar plots of the distribution for the two models described in the text. Panel (c) shows the diabatic population in the S_2 state (solid curve) along with the asymmetry parameters corresponding to the polar plots shown in panels (a) (given as +) and (b) (given as ×). The duration and intensities of the pump and probe pulses are as in Fig. 1. The photoelectron energy is 0.90, 0.40, 0.60, 0.36, and 0.92 eV from left to right, chosen at the peak of the photoelectron distribution.

energy spectrum is accentuated in the energy-resolved asymmetry parameters, where vibrational coherences are filtered out. In the case of model B the sensitivity of the photoelectron image to the electronic population dynamics owes to both the photoelectron symmetry change and its energy change upon transition.

We find that the energy resolution of PEI eliminates a misleading structure that (depending on the ionization dynamics) may be observed in the energy-integrated PAD. Again, depending on details of the ionization dynamics, the energy resolution may also enable the observables of PEI to reflect the population transfer in cases where the energy-integrated PAD fails for symmetry reasons.

Figure 3 illustrates the effect of the pump intensity on the photoelectron image. In order to focus entirely on intensity effects we consider the case where the coupled states correlate with different ion states (model A) and compute the photoelectron signals that would result from the $S_1 \rightarrow I_0$ ionization alone, thus eliminating the effect observed at weak fields [Fig. 2(a)]. (The PEI corresponding to the $S_2 \rightarrow I_1$ ionization contains the same physics and is not shown.) For this model, the asymmetry parameters obtained in a weak field calculation are constant. The structure observed at nonperturbative intensities is entirely due to the rotational interferences that are induced by the electronic transition. As discussed above, rotational excitation in moderately intense fields is sequential, with population in different rotational states

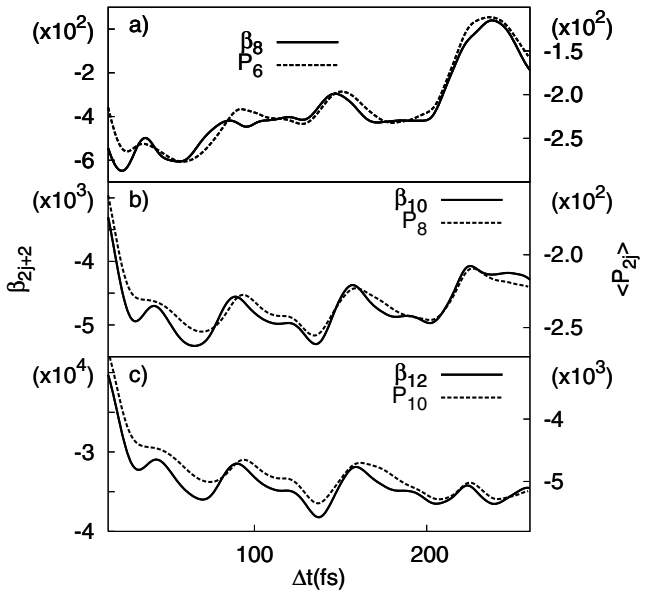

FIG. 3. Energy-resolved asymmetry parameters β_{2j+2} at a fixed photoelectron energy of 2 eV (solid curves) and moments of alignment in the S_1 state $\langle P_{2j}(S_1)\rangle$ for model A (dashed curves). (a) $j = 3$, (b) $j = 4$, and (c) $j = 5$. The pump intensity ($I_{\mathrm{pu}} = 20\ \mathrm{TW\,cm^{-2}}$) and duration ($2\sqrt{\ln 2}\tau_{\mathrm{pu}} = 15$ fs) are chosen to allow several J-exchanging cycles during the pump pulse. The pump and probe energies are as in Fig. 1.

building up with time delays of order few Ω_R^{-1} [18]. Consequently, vibrational wave packets of different angular momenta are transferred to the dark state at different times, resulting in field-induced rotational interferences that are observed as a structure in the asymmetry parameters. As seen in Fig. 3, the structure of β_{2j+2} correlates well with that of the $2j$th moment of the alignment in the S_1 state, $\langle P_{2j}(S_1)\rangle \equiv \langle\psi_{S_1}|P_{2j}|\psi_{S_1}\rangle / \langle\psi_{S_1}|\psi_{S_1}\rangle$, P_{2j} being a Legendre polynomial. Temperature effects, excluded from the present calculation, are expected to simplify the structure of the moments of the alignment and with it the structure of the asymmetry parameters of Fig. 3. These remain to be investigated.

In summary, we reported the first calculation of time-resolved PADs for a polyatomic molecule. Our calculation takes rotations into exact account, treats the field nonperturbatively, and computes the electronic dynamics from first principles. Our results suggest that time-resolved photoelectron images would often contain information that is not available from the combination of (angle-integrated) photoelectron energy distributions and (energy-integrated) photoelectron angular distributions. We illustrated the roles played by the pump pulse intensity and by the energy dependence of the ionization matrix elements.

*Author to whom correspondence should be addressed. Electronic address: tamar.seideman@nrc.ca

[1] For a general review of the field of femtochemistry and a wide variety of applications, see A. H. Zewail, *Femtochemistry: Ultrafast Dynamics of the Chemical Bond* (World Scientific, Singapore, 1994).
[2] For a review of time-resolved photoelectron spectroscopy, see D. M. Neumark, Annu. Rev. Phys. Chem. **52**, 255 (2001).
[3] For a review of the concept, theory, and applications of time-resolved photoelectron angular distributions, see T. Seideman, Annu. Rev. Phys. Chem. **53**, 41 (2002).
[4] For a review of the technique of charged particle imaging, which includes a detailed discussion of time-resolved PEI, see T. Suzuki and B. J. Whitaker, Int. Rev. Phys. Chem. **20**, 313 (2001).
[5] Recent time-resolved PEI experiments are described in T. Suzuki, L. Wang, and H. Kohguchi, J. Chem. Phys. **111**, 4859 (1999); M. Tsubouchi *et al.*, Phys. Rev. Lett. **86**, 4500 (2001); J. K. Song, M. Tsubouchi, and T. Suzuki, J. Chem. Phys. **115**, 8810 (2001); J. A. Davies *et al.*, J. Chem. Phys. **111**, 1 (1999); J. A. Davies *et al.*, Phys. Rev. Lett. **84**, 5983 (2000). The former three articles focus on different problems in the spectroscopy of pyrazine.
[6] For a review of nonadiabatic excited state dynamics as probed by time-resolved photoelectron spectroscopy, see C. C. Hayden and A. Stolow, in *Photoionization and Photodetachment*, edited by C.-Y. Ng, Advanced Series in Physical Chemistry Vol. 10A (World Scientific, Singapore, River Edge, NJ, 1999), p. 91. Brief updates are found in [2,3].
[7] T. Seideman, J. Chem. Phys. **107**, 7859 (1997).
[8] T. Seideman, Phys. Rev. A **64**, 042504 (2001).
[9] V. Blanchet, M. Zgierski, T. Seideman, and A. Stolow, Nature (London) **401**, 52 (1999).
[10] D. Toffoli *et al.*, Chem. Phys. **276**, 25 (2002).
[11] W. Domcke and G. Stock, in *Theory of Ultrafast Nonadiabatic Excited-State Processes and Their Spectroscopic Detection in Real Time*, edited by I. Prigogine and S. A. Rice, Advanced Series in Chemical Physics Vol. 100 (John Wiley & Sons, New York, 1997), and references therein.
[12] M. Seel and W. Domcke, J. Chem. Phys. **95**, 7806 (1991).
[13] In this work we use the potential surfaces of Refs. [14,15], which differ somewhat from those of Ref. [12].
[14] L. Seidner, W. Domcke, and W. von Niessen, Chem. Phys. Lett. **205**, 117 (1993).
[15] G. Stock *et al.*, J. Chem. Phys. **103**, 6851 (1995).
[16] V. Stert, P. Farmanara, and W. Radloff, J. Chem. Phys. **112**, 4460 (2000).
[17] S. Hahn and G. Stock, Phys. Chem. Chem. Phys. **3**, 2331 (2001).
[18] T. Seideman, J. Chem. Phys. **103**, 7887 (1995); Phys. Rev. Lett. **83**, 4971 (1999).
[19] T. Seideman, J. Chem. Phys. **113**, 1677 (2000).
[20] C. C. Hayden (unpublished).
[21] J. J. Larsen *et al.*, Phys. Rev. Lett. **85**, 2470 (2000).